

Damping signatures at JUNO, a medium-baseline reactor neutrino oscillation experiment

Jun Wang¹ Jiajun Liao^{*1} Wei Wang^{†1} Angel Abusleme⁶ Thomas Adam⁴⁵ Shakeel Ahmad⁶⁶ Rizwan Ahmed⁶⁶ Sebastiano Aiello⁵⁵ Muhammad Akram⁶⁶ Fengpeng An²⁹ Qi An²² Giuseppe Andronico⁵⁵ Nikolay Anfimov⁶⁷ Vito Antonelli⁵⁷ Tatiana Antoshkina⁶⁷ Burin Asavapibhop⁷¹ João Pedro Athayde Marcondes de André⁴⁵ Didier Auguste⁴³ Andrej Babic⁷⁰ Nikita Balashov⁶⁷ Wander Baldini⁵⁶ Andrea Barresi⁵⁸ Davide Basilico⁵⁷ Eric Baussan⁴⁵ Marco Bellato⁶⁰ Antonio Bergnoli⁶⁰ Thilo Birkenfeld⁴⁸ Sylvie Blin⁴³ David Blum⁵⁴ Simon Blyth⁴⁰ Anastasia Bolshakova⁶⁷ Mathieu Bongrand⁴⁷ Clément Bordereau^{44,40} Dominique Breton⁴³ Augusto Brigatti⁵⁷ Riccardo Brugnera⁶¹ Riccardo Bruno⁵⁵ Antonio Budano⁶⁴ Mario Buscemi⁵⁵ Jose Busto⁴⁶ Ilya Butorov⁶⁷ Anatael Cabrera⁴³ Hao Cai³⁴ Xiao Cai¹¹ Yanke Cai¹¹ Zhiyan Cai¹¹ Riccardo Callegari⁶¹ Antonio Cammi⁵⁹ Agustin Campeny⁶ Chuanya Cao¹¹ Guofu Cao¹¹ Jun Cao¹¹ Rossella Caruso⁵⁵ Cédric Cerna⁴⁴ Jinfan Chang¹¹ Yun Chang³⁹ Pingping Chen¹⁹ Po-An Chen⁴⁰ Shaomin Chen¹⁴ Xurong Chen²⁶ Yi-Wen Chen³⁸ Yixue Chen¹² Yu Chen¹ Zhang Chen¹¹ Jie Cheng¹¹ Yaping Cheng⁸ Alexey Chetverikov⁶⁷ Davide Chiesa⁵⁸ Pietro Chimenti⁴ Artem Chukanov⁶⁷ Gérard Claverie⁴⁴ Catia Clementi⁶² Barbara Clerbaux³ Selma Conforti Di Lorenzo⁴⁴ Daniele Corti⁶⁰ Flavio Dal Corso⁶⁰ Olivia Dalager⁷⁴ Christophe De La Taille⁴⁴ Jiawei Deng³⁴ Zhi Deng¹⁴ Ziyang Deng¹¹ Wilfried Depnering⁵² Marco Diaz⁶ Xuefeng Ding⁵⁷ Yayun Ding¹¹ Bayu Dirgantara⁷³ Sergey Dmitrievsky⁶⁷ Tadeas Dohnal⁴¹ Dmitry Dolzhikov⁶⁷ Georgy Donchenko⁶⁹ Jianmeng Dong¹⁴ Evgeny Doroshkevich⁶⁸ Marcos Dracos⁴⁵ Frédéric Druillolle⁴⁴ Ran Du¹¹ Shuxian Du³⁷ Stefano Dusini⁶⁰ Martin Dvorak⁴¹ Timo Enqvist⁴² Heike Enzmann⁵² Andrea Fabbri⁶⁴ Lukas Fajt⁷⁰ Donghua Fan²⁴ Lei Fan¹¹ Jian Fang¹¹ Wenxing Fang¹¹ Marco Fargetta⁵⁵ Dmitry Fedoseev⁶⁷ Vladko Fekete⁷⁰ Li-Cheng Feng³⁸ Qichun Feng²¹ Richard Ford⁵⁷ Amélie Fournier⁴⁴ Haonan Gan³² Feng Gao⁴⁸ Alberto Garfagnini⁶¹ Arsenii Gavrikov⁶¹ Marco Giammarchi⁵⁷ Agnese Giaz⁶¹ Nunzio Giudice⁵⁵ Maxim Gonchar⁶⁷ Guanghua Gong¹⁴ Hui Gong¹⁴ Yuri Gornushkin⁶⁷ Alexandre Göttel^{50,48} Marco Grassi⁶¹ Christian Grewing⁵¹ Vasily Gromov⁶⁷ Minghao Gu¹¹ Xiaofei Gu³⁷ Yu Gu²⁰ Mengyun Guan¹¹ Nunzio Guardone⁵⁵ Maria Gul⁶⁶ Cong Guo¹¹ Jingyuan Guo¹ Wanlei Guo¹¹ Xinheng Guo⁹ Yuhang Guo^{35,50} Paul Hackspacher⁵² Caren Hagner⁴⁹ Ran Han⁸ Yang Han¹ Muhammad Sohaib Hassan⁶⁶ Miao He¹¹ Wei He¹¹ Tobias Heinz⁵⁴ Patrick Hellmuth⁴⁴ Yuekun Heng¹¹ Rafael Herrera⁶ YuenKeung Hor¹ Shaojing Hou¹¹ Yee Hsiung⁴⁰ Bei-Zhen Hu⁴⁰ Hang Hu¹ Jianrun Hu¹¹ Jun Hu¹¹ Shouyang Hu¹⁰ Tao Hu¹¹ Zhuojun Hu¹ Chunhao Huang¹ Guihong Huang¹¹ Hanxiang Huang¹⁰ Wenhao Huang²⁵ Xin Huang¹¹ Xingtao Huang²⁵ Yongbo Huang²⁸ Jiaqi Hui³⁰ Lei

*Corresponding author.

†Corresponding author.

Huo²¹ Wenju Huo²² Cédric Huss⁴⁴ Safer Hussain⁶⁶ Ara Ioannisian² Roberto Isocrate⁶⁰
Beatrice Jelmini⁶¹ Kuo-Lun Jen³⁸ Ignacio Jeria⁶ Xiaolu Ji¹¹ Xingzhao Ji¹ Huihui Jia³³ Junji
Jia³⁴ Siyu Jian¹⁰ Di Jiang²² Wei Jiang¹¹ Xiaoshan Jiang¹¹ Ruyi Jin¹¹ Xiaoping Jing¹¹ Cécile
Jollet⁴⁴ Jari Joutsenvaara⁴² Sirichok Jungthawan⁷³ Leonidas Kalousis⁴⁵ Philipp
Kampmann⁵⁰ Li Kang¹⁹ Rebin Karaparambil⁴⁷ Narine Kazarian² Khanchai
Khosonthongkee⁷³ Denis Korablev⁶⁷ Konstantin Kouzakov⁶⁹ Alexey Krasnoperov⁶⁷ Andre
Kruth⁵¹ Nikolay Kutovskiy⁶⁷ Pasi Kuusiniemi⁴² Tobias Lachenmaier⁵⁴ Cecilia Landini⁵⁷
Sébastien Leblanc⁴⁴ Victor Lebrin⁴⁷ Frederic Lefevre⁴⁷ Ruiting Lei¹⁹ Rupert Leitner⁴¹ Jason
Leung³⁸ Demin Li³⁷ Fei Li¹¹ Fule Li¹⁴ Haitao Li¹ Huiling Li¹¹ Jiaqi Li¹ Mengzhao Li¹¹ Min
Li¹² Nan Li¹¹ Nan Li¹⁷ Qingjiang Li¹⁷ Ruhui Li¹¹ Shanfeng Li¹⁹ Tao Li¹ Weidong Li^{11,15}
Weiguo Li¹¹ Xiaomei Li¹⁰ Xiaonan Li¹¹ Xinglong Li¹⁰ Yi Li¹⁹ Yufeng Li¹¹ Zhaohan Li¹¹
Zhibing Li¹ Ziyuan Li¹ Hao Liang¹⁰ Hao Liang²² Daniel Liebau⁵¹ Ayut Limphirat⁷³ Sukit
Limpijumng⁷³ Guey-Lin Lin³⁸ Shengxin Lin¹⁹ Tao Lin¹¹ Jiajie Ling¹ Ivano Lippi⁶⁰ Fang
Liu¹² Haidong Liu³⁷ Hongbang Liu²⁸ Hongjuan Liu²³ Hongtao Liu¹ Hui Liu²⁰ Jianglai
Liu^{30,31} Jinchang Liu¹¹ Min Liu²³ Qian Liu¹⁵ Qin Liu²² Runxuan Liu^{50,48} Shuangyu Liu¹¹
Shubin Liu²² Shulin Liu¹¹ Xiaowei Liu¹ Xiwen Liu²⁸ Yan Liu¹¹ Yunzhe Liu¹¹ Alexey
Lokhov^{69,68} Paolo Lombardi⁵⁷ Claudio Lombardo⁵⁵ Kai Loo⁵² Chuan Lu³² Haoqi Lu¹¹
Jingbin Lu¹⁶ Janguang Lu¹¹ Shuxiang Lu³⁷ Xiaoxu Lu¹¹ Bayarto Lubsandorzhev⁶⁸ Sultim
Lubsandorzhev⁶⁸ Livia Ludhova^{50,48} Arslan Lukanov⁶⁸ Fengjiao Luo¹¹ Guang Luo¹ Pengwei
Luo¹ Shu Luo³⁶ Wuming Luo¹¹ Vladimir Lyashuk⁶⁸ Bangzheng Ma²⁵ Qiumei Ma¹¹ Si Ma¹¹
Xiaoyan Ma¹¹ Xubo Ma¹² Jihane Maalmi⁴³ Yury Malyskin⁶⁷ Roberto Carlos Mandujano⁷⁴
Fabio Mantovani⁵⁶ Francesco Manzali⁶¹ Xin Mao⁸ Yajun Mao¹³ Stefano M. Mari⁶⁴ Filippo
Marini⁶¹ Sadia Marium⁶⁶ Cristina Martellini⁶⁴ Gisele Martin-Chassard⁴³ Agnese Martini⁶³
Matthias Mayer⁵³ Davit Mayilyan² Ints Mednieks⁶⁵ Yue Meng³⁰ Anselmo Meregaglia⁴⁴
Emanuela Meroni⁵⁷ David Meyhöfer⁴⁹ Mauro Mezzetto⁶⁰ Jonathan Miller⁷ Lino
Miramonti⁵⁷ Paolo Montini⁶⁴ Michele Montuschi⁵⁶ Axel Müller⁵⁴ Massimiliano Nastasi⁵⁸
Dmitry V. Naumov⁶⁷ Elena Naumova⁶⁷ Diana Navas-Nicolas⁴³ Igor Nemchenok⁶⁷ Minh
Thuan Nguyen Thi³⁸ Feipeng Ning¹¹ Zhe Ning¹¹ Hiroshi Nunokawa⁵ Lothar Oberauer⁵³
Juan Pedro Ochoa-Ricoux^{74,5} Alexander Olshevskiy⁶⁷ Domizia Orestano⁶⁴ Fausto Ortica⁶²
Rainer Othegraven⁵² Hsiao-Ru Pan⁴⁰ Alessandro Paoloni⁶³ Sergio Parmeggiano⁵⁷ Yatian
Pei¹¹ Nicomede Pelliccia⁶² Anguo Peng²³ Haiping Peng²² Frédéric Perrot⁴⁴
Pierre-Alexandre Petitjean³ Fabrizio Petrucci⁶⁴ Oliver Pilarczyk⁵² Luis Felipe Piñeres Rico⁴⁵
Artyom Popov⁶⁹ Pascal Poussot⁴⁵ Wathan Pratumwan⁷³ Ezio Previtali⁵⁸ Fazhi Qi¹¹ Ming
Qi²⁷ Sen Qian¹¹ Xiaohui Qian¹¹ Zhen Qian¹ Hao Qiao¹³ Zhonghua Qin¹¹ Shoukang Qiu²³
Muhammad Usman Rajput⁶⁶ Gioacchino Ranucci⁵⁷ Neill Raper¹ Alessandra Re⁵⁷ Henning
Rebber⁴⁹ Abdel Rebi⁴⁴ Bin Ren¹⁹ Jie Ren¹⁰ Barbara Ricci⁵⁶ Markus Robens⁵¹ Mathieu
Roche⁴⁴ Narongkiat Rodphai⁷¹ Aldo Romani⁶² Bedřich Roskovec⁴¹ Christian Roth⁵¹
Xiangdong Ruan²⁸ Xichao Ruan¹⁰ Saroj Rujirawat⁷³ Arseniy Rybnikov⁶⁷ Andrey Sadovsky⁶⁷
Paolo Saggese⁵⁷ Simone Sanfilippo⁶⁴ Anut Sangka⁷² Nuanwan Sanguansak⁷³ Utane
Sawangwit⁷² Julia Sawatzki⁵³ Fatma Sawy⁶¹ Michaela Schever^{50,48} Cédric Schwab⁴⁵
Konstantin Schweizer⁵³ Alexandr Selyunin⁶⁷ Andrea Serafini⁵⁶ Giulio Settanta⁵⁰ Mariangela
Settimo⁴⁷ Zhuang Shao³⁵ Vladislav Sharov⁶⁷ Arina Shaydurova⁶⁷ Jingyan Shi¹¹ Yanan Shi¹¹
Vitaly Shutov⁶⁷ Andrey Sidorenkov⁶⁸ Fedor Šimkovic⁷⁰ Chiara Sirignano⁶¹ Jaruchit Siripak⁷³

Monica Sisti⁵⁸ Maciej Slupecki⁴² Mikhail Smirnov¹ Oleg Smirnov⁶⁷ Thiago Sogo-Bezerra⁴⁷
 Sergey Sokolov⁶⁷ Julanan Songwadhana⁷³ Boonrucksar Soonthornthum⁷² Albert Sotnikov⁶⁷
 Ondřej Šrámek⁴¹ Warintorn Sreethawong⁷³ Achim Stahl⁴⁸ Luca Stanco⁶⁰ Konstantin
 Stankevich⁶⁹ Dušan Štefánik⁷⁰ Hans Steiger^{52,53} Jochen Steinmann⁴⁸ Tobias Sterr⁵⁴
 Matthias Raphael Stock⁵³ Virginia Strati⁵⁶ Alexander Studenikin⁶⁹ Shifeng Sun¹² Xilei
 Sun¹¹ Yongjie Sun²² Yongzhao Sun¹¹ Narumon Suwonjandee⁷¹ Michal Szelezniak⁴⁵ Jian
 Tang¹ Qiang Tang¹ Quan Tang²³ Xiao Tang¹¹ Alexander Tietzsch⁵⁴ Igor Tkachev⁶⁸ Tomas
 Tmej⁴¹ Marco Danilo Claudio Torri⁴¹ Konstantin Treskov⁶⁷ Andrea Triossi⁴⁵ Giancarlo
 Troni⁶ Wladyslaw Trzaska⁴² Cristina Tuve⁵⁵ Nikita Ushakov⁶⁸ Johannes van den Boom⁵¹
 Stefan van Waasen⁵¹ Guillaume Vanroyen⁴⁷ Vadim Vedin⁶⁵ Giuseppe Verde⁵⁵ Maxim
 Vialkov⁶⁹ Benoit Viaud⁴⁷ Cornelius Moritz Vollbrecht^{50,48} Cristina Volpe⁴³ Vit Vorobel⁴¹
 Dmitriy Voronin⁶⁸ Lucia Votano⁶³ Pablo Walker⁶ Caishen Wang¹⁹ Chung-Hsiang Wang³⁹ En
 Wang³⁷ Guoli Wang²¹ Jian Wang²² Kunyu Wang¹¹ Lu Wang¹¹ Meifen Wang¹¹ Meng
 Wang²³ Meng Wang²⁵ Ruiguang Wang¹¹ Siguang Wang¹³ Wei Wang²⁷ Wenshuai Wang¹¹
 Xi Wang¹⁷ Xiangyue Wang¹ Yangfu Wang¹¹ Yaoguang Wang¹¹ Yi Wang¹⁴ Yi Wang²⁴
 Yifang Wang¹¹ Yuanqing Wang¹⁴ Yuman Wang²⁷ Zhe Wang¹⁴ Zheng Wang¹¹ Zhimin
 Wang¹¹ Zongyi Wang¹⁴ Muhammad Waqas⁶⁶ Apimook Watcharangkool⁷² Lianghong Wei¹¹
 Wei Wei¹¹ Wenlu Wei¹¹ Yadong Wei¹⁹ Kaile Wen¹¹ Liangjian Wen¹¹ Christopher
 Wiebusch⁴⁸ Steven Chan-Fai Wong¹ Bjoern Wonsak⁴⁹ Diru Wu¹¹ Qun Wu²⁵ Zhi Wu¹¹
 Michael Wurm⁵² Jacques Wurtz⁴⁵ Christian Wysotzki⁴⁸ Yufei Xi³² Dongmei Xia¹⁸
 Xiaochuan Xie¹⁸ Yuguang Xie¹¹ Zhangquan Xie¹¹ Zhizhong Xing¹¹ Benda Xu¹⁴ Cheng Xu²³
 Donglian Xu^{31,30} Fanrong Xu²⁰ Hangkun Xu¹¹ Jilei Xu¹¹ Jing Xu⁹ Meihang Xu¹¹ Yin Xu³³
 Yu Xu^{50,48} Baojun Yan¹¹ Taylor Yan⁷³ Wenqi Yan¹¹ Xiongbo Yan¹¹ Yupeng Yan⁷³ Anbo
 Yang¹¹ Changgen Yang¹¹ Chengfeng Yang²⁸ Huan Yang¹¹ Jie Yang³⁷ Lei Yang¹⁹ Xiaoyu
 Yang¹¹ Yifan Yang¹¹ Yifan Yang³ Haifeng Yao¹¹ Zafar Yasin⁶⁶ Jiaxuan Ye¹¹ Mei Ye¹¹ Ziping
 Ye³¹ Ugur Yegin⁵¹ Frédéric Yermia⁴⁷ Peihuai Yi¹¹ Na Yin²⁵ Xiangwei Yin¹¹ Zhengyun You¹
 Boxiang Yu¹¹ Chiye Yu¹⁹ Chunxu Yu³³ Hongzhao Yu¹ Miao Yu³⁴ Xianghui Yu³³ Zeyuan Yu¹¹
 Zezhong Yu¹¹ Chengzhuo Yuan¹¹ Ying Yuan¹³ Zhenxiang Yuan¹⁴ Ziyi Yuan³⁴ Baobiao Yue¹
 Noman Zafar⁶⁶ Andre Zambanini⁵¹ Vitalii Zavadskiy⁶⁷ Shan Zeng¹¹ Tingxuan Zeng¹¹ Yuda
 Zeng¹ Liang Zhan¹¹ Aiqiang Zhang¹⁴ Feiyang Zhang³⁰ Guoqing Zhang¹¹ Haiqiong Zhang¹¹
 Honghao Zhang¹ Jiawen Zhang¹¹ Jie Zhang¹¹ Jin Zhang²⁸ Jingbo Zhang²¹ Jinnan Zhang¹¹
 Peng Zhang¹¹ Qingmin Zhang³⁵ Shiqi Zhang¹ Shu Zhang¹ Tao Zhang³⁰ Xiaomei Zhang¹¹
 Xuantong Zhang¹¹ Xueyao Zhang²⁵ Yan Zhang¹¹ Yinhong Zhang¹¹ Yiyu Zhang¹¹ Yongpeng
 Zhang¹¹ Yuanyuan Zhang³⁰ Yumei Zhang¹ Zhenyu Zhang³⁴ Zhijian Zhang¹⁹ Fengyi Zhao²⁶
 Jie Zhao¹¹ Rong Zhao¹ Shujun Zhao³⁷ Tianchi Zhao¹¹ Dongqin Zheng²⁰ Hua Zheng¹⁹
 Minshan Zheng¹⁰ Yangheng Zheng¹⁵ Weirong Zhong²⁰ Jing Zhou¹⁰ Li Zhou¹¹ Nan Zhou²²
 Shun Zhou¹¹ Tong Zhou¹¹ Xiang Zhou³⁴ Jiang Zhu¹ Kangfu Zhu³⁵ Kejun Zhu¹¹ Zhihang
 Zhu¹¹ Bo Zhuang¹¹ Honglin Zhuang¹¹ Liang Zong¹⁴ Jiaheng Zou¹¹

¹ Sun Yat-Sen University, Guangzhou, China

² Yerevan Physics Institute, Yerevan, Armenia

³ Université Libre de Bruxelles, Brussels, Belgium

⁴ Universidade Estadual de Londrina, Londrina, Brazil

⁵ Pontificia Universidade Catolica do Rio de Janeiro, Rio, Brazil

- ⁶*Pontificia Universidad Católica de Chile, Santiago, Chile*
- ⁷*Universidad Tecnica Federico Santa Maria, Valparaiso, Chile*
- ⁸*Beijing Institute of Spacecraft Environment Engineering, Beijing, China*
- ⁹*Beijing Normal University, Beijing, China*
- ¹⁰*China Institute of Atomic Energy, Beijing, China*
- ¹¹*Institute of High Energy Physics, Beijing, China*
- ¹²*North China Electric Power University, Beijing, China*
- ¹³*School of Physics, Peking University, Beijing, China*
- ¹⁴*Tsinghua University, Beijing, China*
- ¹⁵*University of Chinese Academy of Sciences, Beijing, China*
- ¹⁶*Jilin University, Changchun, China*
- ¹⁷*College of Electronic Science and Engineering, National University of Defense Technology, Changsha, China*
- ¹⁸*Chongqing University, Chongqing, China*
- ¹⁹*Dongguan University of Technology, Dongguan, China*
- ²⁰*Jinan University, Guangzhou, China*
- ²¹*Harbin Institute of Technology, Harbin, China*
- ²²*University of Science and Technology of China, Hefei, China*
- ²³*The Radiochemistry and Nuclear Chemistry Group in University of South China, Hengyang, China*
- ²⁴*Wuyi University, Jiangmen, China*
- ²⁵*Shandong University, Jinan, China, and Key Laboratory of Particle Physics and Particle Irradiation of Ministry of Education, Shandong University, Qingdao, China*
- ²⁶*Institute of Modern Physics, Chinese Academy of Sciences, Lanzhou, China*
- ²⁷*Nanjing University, Nanjing, China*
- ²⁸*Guangxi University, Nanning, China*
- ²⁹*East China University of Science and Technology, Shanghai, China*
- ³⁰*School of Physics and Astronomy, Shanghai Jiao Tong University, Shanghai, China*
- ³¹*Tsung-Dao Lee Institute, Shanghai Jiao Tong University, Shanghai, China*
- ³²*Institute of Hydrogeology and Environmental Geology, Chinese Academy of Geological Sciences, Shijiazhuang, China*
- ³³*Nankai University, Tianjin, China*
- ³⁴*Wuhan University, Wuhan, China*
- ³⁵*Xi'an Jiaotong University, Xi'an, China*
- ³⁶*Xiamen University, Xiamen, China*
- ³⁷*School of Physics and Microelectronics, Zhengzhou University, Zhengzhou, China*
- ³⁸*Institute of Physics, National Yang Ming Chiao Tung University, Hsinchu*
- ³⁹*National United University, Miao-Li*
- ⁴⁰*Department of Physics, National Taiwan University, Taipei*
- ⁴¹*Charles University, Faculty of Mathematics and Physics, Prague, Czech Republic*
- ⁴²*University of Jyväskylä, Department of Physics, Jyväskylä, Finland*
- ⁴³*IJCLab, Université Paris-Saclay, CNRS/IN2P3, 91405 Orsay, France*
- ⁴⁴*Univ. Bordeaux, CNRS, LP2i Bordeaux, UMR 5797, F-33170 Gradignan, France*
- ⁴⁵*IPHC, Université de Strasbourg, CNRS/IN2P3, F-67037 Strasbourg, France*
- ⁴⁶*Aix-Marseille Univ, CNRS/IN2P3, CPPM, Marseille, France*

- ⁴⁷*SUBATECH, Nantes Université, IMT Atlantique, CNRS-IN2P3, Nantes, France*
- ⁴⁸*III. Physikalisches Institut B, RWTH Aachen University, Aachen, Germany*
- ⁴⁹*Institute of Experimental Physics, University of Hamburg, Hamburg, Germany*
- ⁵⁰*Forschungszentrum Jülich GmbH, Nuclear Physics Institute IKP-2, Jülich, Germany*
- ⁵¹*Forschungszentrum Jülich GmbH, Central Institute of Engineering, Electronics and Analytics - Electronic Systems (ZEA-2), Jülich, Germany*
- ⁵²*Institute of Physics, Johannes-Gutenberg Universität Mainz, Mainz, Germany*
- ⁵³*Technische Universität München, München, Germany*
- ⁵⁴*Eberhard Karls Universität Tübingen, Physikalisches Institut, Tübingen, Germany*
- ⁵⁵*INFN Catania and Dipartimento di Fisica e Astronomia dell'Università di Catania, Catania, Italy*
- ⁵⁶*Department of Physics and Earth Science, University of Ferrara and INFN Sezione di Ferrara, Ferrara, Italy*
- ⁵⁷*INFN Sezione di Milano and Dipartimento di Fisica dell'Università di Milano, Milano, Italy*
- ⁵⁸*INFN Milano Bicocca and University of Milano Bicocca, Milano, Italy*
- ⁵⁹*INFN Milano Bicocca and Politecnico di Milano, Milano, Italy*
- ⁶⁰*INFN Sezione di Padova, Padova, Italy*
- ⁶¹*Dipartimento di Fisica e Astronomia dell'Università di Padova and INFN Sezione di Padova, Padova, Italy*
- ⁶²*INFN Sezione di Perugia and Dipartimento di Chimica, Biologia e Biotecnologie dell'Università di Perugia, Perugia, Italy*
- ⁶³*Laboratori Nazionali di Frascati dell'INFN, Roma, Italy*
- ⁶⁴*University of Roma Tre and INFN Sezione Roma Tre, Roma, Italy*
- ⁶⁵*Institute of Electronics and Computer Science, Riga, Latvia*
- ⁶⁶*Pakistan Institute of Nuclear Science and Technology, Islamabad, Pakistan*
- ⁶⁷*Joint Institute for Nuclear Research, Dubna, Russia*
- ⁶⁸*Institute for Nuclear Research of the Russian Academy of Sciences, Moscow, Russia*
- ⁶⁹*Lomonosov Moscow State University, Moscow, Russia*
- ⁷⁰*Comenius University Bratislava, Faculty of Mathematics, Physics and Informatics, Bratislava, Slovakia*
- ⁷¹*Department of Physics, Faculty of Science, Chulalongkorn University, Bangkok, Thailand*
- ⁷²*National Astronomical Research Institute of Thailand, Chiang Mai, Thailand*
- ⁷³*Suranaree University of Technology, Nakhon Ratchasima, Thailand*
- ⁷⁴*Department of Physics and Astronomy, University of California, Irvine, California, USA*

ABSTRACT: We study damping signatures at the Jiangmen Underground Neutrino Observatory (JUNO), a medium-baseline reactor neutrino oscillation experiment. These damping signatures are motivated by various new physics models, including quantum decoherence, ν_3 decay, neutrino absorption, and wave packet decoherence. The phenomenological effects of these models can be characterized by exponential damping factors at the probability level. We assess how well JUNO can constrain these damping parameters and how to disentangle these different damping signatures at JUNO. Compared to current experimental limits, JUNO can significantly improve the limits on τ_3/m_3 in the ν_3 decay model, the width of the neutrino wave packet σ_x , and the intrinsic relative dispersion of neutrino momentum σ_{rel} .

Contents

1	Introduction	1
2	Damping signatures from new physics models	2
3	Damping signatures at medium-baseline reactor neutrino experiments	5
3.1	Damped neutrino oscillation probabilities	5
3.2	Classification of damping effects	7
4	Analysis method for JUNO	9
5	Results	10
5.1	Constraints on the damping parameters at JUNO	10
5.2	Disentangling damping signatures at JUNO	12
6	Conclusions	14

1 Introduction

Neutrino oscillation was first proposed by Bruno Pontecovero in 1957 [1] and was invoked for the solution of atmospheric neutrino anomaly and solar neutrino puzzle. It was experimentally confirmed by the Super-Kamioka Neutrino Detection Experiment (Super-K, SK) [2] in 1998 and the Sudbury Neutrino Observatory (SNO) [3] in 2002; for further details see Ref. [4]. Most neutrino oscillation experiments can be well explained in the Standard Model (SM) with three massive neutrinos. In the standard three-flavor neutrino oscillation framework, the three known neutrino flavor eigenstates (ν_e , ν_μ , and ν_τ) can be written as quantum superpositions of three mass eigenstates (ν_1 , ν_2 , and ν_3), and the neutrino oscillation probabilities are expressed in terms of six oscillation parameters: three mixing angles (θ_{12} , θ_{13} , and θ_{23}), two mass-squared differences (Δm_{21}^2 and Δm_{31}^2), and one Dirac CP phase (δ_{CP}). The Majorana CP phases play no role in neutrino oscillations if neutrinos are Majorana particles. Among these six observable oscillation parameters, Δm_{21}^2 , $|\Delta m_{31}^2|$, θ_{12} , and θ_{13} have been well determined to the few-percent level. However, the neutrino mass ordering (whether Δm_{31}^2 is positive or negative), the octant of θ_{23} (whether θ_{23} is larger or smaller than 45°) and the Dirac CP phase are still open questions. At present, the normal mass ordering (NMO) and the second octant of θ_{23} are both favored by less than 3σ confidence level (CL) [4–6], and δ_{CP} is in the range of $[-3.41, -0.03]$ for the NMO and $[-2.54, -0.32]$ for the inverted mass ordering (IMO) at the 3σ CL [7], respectively. The main physics goals of next-generation neutrino oscillation experiments, such as the Deep Underground Neutrino Experiment (DUNE) [8, 9], Hyper-Kamiokande [10] and the Jiangmen Underground Neutrino Observatory (JUNO) [11, 12], are to determine the mass ordering with a $3-5\sigma$ CL and to observe CP violation with a 3σ CL for $\sim 75\%$ of δ_{CP} values, etc. To reach these

goals, the ability to achieve high-precision measurement of the oscillation spectrum is required for these experiments. In the meantime, these high-precision experiments will also reach sufficient sensitivity to probe new physics beyond the standard three-neutrino paradigm.

The presence of new physics in the neutrino sector would yield corrections to the standard three-flavor neutrino oscillation probabilities, thus leading to modifications to the spectrum measured in high-precision neutrino oscillation experiments. Among various possible new physics scenarios, a number of them lead to exponential damping in the neutrino oscillation probabilities [13, 14], which could yield a different number of neutrinos observed than expected [14–19] or a shift in the best fit values for neutrino oscillation parameters [13–17, 20–25]. These damping signatures can be treated as secondary effects relative to the standard three-neutrino oscillations in the neutrino flavor transitions. In this work, we present a systematic study of the possible damping effects at the JUNO detector. JUNO is a medium-baseline reactor neutrino experiment with a 20kton liquid scintillator (LS) detector located in a laboratory at 700m underground in Jiangmen, China. The main physics goals of JUNO are to determine the mass ordering and perform high-precision measurements of the neutrino oscillation parameters $\sin^2 \theta_{12}$, Δm_{21}^2 and $|\Delta m_{ee}^2|$ [11, 12]. Also, JUNO is expected to be sensitive to the tiny damping signatures due to its effective energy resolution of 3% at 1 MeV and the capability of measuring multiple oscillation cycles [25].

This paper is organized as follows. In Section 2, we discuss the damping signatures arising from different new physics models. In Section 3, we discuss the damping signatures at medium-baseline reactor neutrino experiments. In Section 4, we describe the statistical analysis method for JUNO used in this work. In Section 5, we present the results of constraining and disentangling damping signatures at JUNO. We conclude in Section 6.

2 Damping signatures from new physics models

Damping signatures can be induced by a class of new physics models. Here, we focus on the exponential damping framework [13, 14], i.e., they can be written in the form of multiplying each term of the neutrino oscillation probabilities with exponential factors, which can arise from an approximation of the first- or second-order perturbations to the standard neutrino oscillation probabilities from new physics scenarios [25–27]. In this framework, the general expression for the probability of ν_a oscillating into ν_b in vacuum is given by

$$P(\nu_a \rightarrow \nu_b) = \sum_{i,j=1}^3 U_{aj} U_{bj}^* U_{ai}^* U_{bi} \exp\left(-i \frac{\Delta m_{ij}^2 L}{2E}\right) D_{ij}(\alpha_{ij}), \quad (2.1)$$

where U is the Pontecorvo-Maki-Nakagawa-Sakata (PMNS) mixing matrix [3, 4], $\Delta m_{ij}^2 = m_i^2 - m_j^2$, with m_i being the eigenstate mass of ν_i ; L is the baseline length, E is the neutrino energy; D_{ij} is an exponential damping factor and the specific form can be found in Table 1, and the α_{ij} are damping coefficients. Hereinafter, except for the ν_3 decay case, we assume universal couplings, i.e., $\alpha_{ij} \equiv \alpha$, to describe the magnitudes of different damping effects.

The damping signatures from various new physics models are summarized in Table 1. These models include quantum decoherence (QD), neutrino absorption, ν_3 decay, and wave packet

Type	Damping effect	Reference	Damping factor D_{ij}	Units of α
(1)	QD I	[20, 23, 28–33]	$\exp(-\alpha L/E^2)$	$\text{MeV}^2 \cdot \text{m}^{-1}$
(2)	QD II	[20, 23, 28–40]	$\exp(-\alpha L)$	m^{-1}
(3)	QD III	[13, 20, 23, 28–33, 35–39]	$\exp(-\alpha LE^2)$	$\text{MeV}^{-2} \cdot \text{m}^{-1}$
(4)	Absorption	[13, 20, 23, 28–32, 40]	$\exp(-\alpha LE)$	$\text{MeV}^{-1} \cdot \text{m}^{-1}$
(5)	ν_3 decay	[15–17, 19, 41–43]	$\{\exp(-\alpha \frac{L}{E}), \exp(-\alpha \frac{L}{2E})\}$	$\text{MeV} \cdot \text{m}^{-1}$
(6)	WPD I	[13, 23, 24, 44–49]	$\exp\left(-\alpha \frac{(\Delta m_{ij}^2)^2 L^2}{E^4}\right)$	MeV^2
(7)	WPD II	[13, 25, 37, 50]	$\exp\left(-\alpha \frac{(\Delta m_{ij}^2)^2 L^2}{E^2}\right)$	dimensionless
(8)	WPD III	[21, 22, 25, 51, 52]	$\exp(-R - \mathbf{iX})$	dimensionless

Table 1: List of new physics models with different exponential damping factors. The definitions of the parameters in the type (8) model are given in Eq. (2.2).

decoherence (WPD). The new physics models of types (1) - (5) in Table 1 are expressed as power-law dependencies of the exponential form, i.e., $\exp(-\alpha LE^n)$ with $n = 0, \pm 1$, and ± 2 [20, 23, 28–33, 35, 37, 39, 40]. Specifically, the type (1) model ($n = -2$) is demonstrated in Ref. [20] that it has the same functional form as the effects induced by stochastic density fluctuations. Thus, it is used to probe QD effects that might be induced by matter density fluctuations. The corresponding constraints of this model can be interpreted as limits on possible matter density fluctuations in the Sun [20]. The most significant feature of the type (2) model ($n = 0$) is independent of neutrino energy. Many researchers have focused on this model since it is the simplest case of QD effects that might be induced by quantum gravity [20, 23, 28–40]. The type (3) model ($n = 2$) is used to probe QD effects that might be induced by the space-time “foam” configurations of quantum gravity or D-brane of the form $\alpha \propto E^2/M_{\text{Planck}}$ [20, 35, 53, 54], where M_{Planck} is the Planck mass scale. The type (4) model ($n = 1$), which is called neutrino absorption in Ref. [13], is used to describe the absorption effect when neutrinos propagate through matter. In this type of model, $\alpha \equiv \rho\sigma(E_0)/E_0$, where ρ is the matter density and $\sigma(E_0)$ is the effective cross section for neutrinos with an energy of E_0 . Currently, neither atmospheric, solar neutrino oscillation experiments nor the long-baseline reactor neutrino experiment Kamioka Liquid Scintillator Anti-Neutrino Detector (KamLAND) shows evidence in favor of the new physics effects described by the previous four models ($n = 0, 1$ and ± 2) [20, 35], which also indicates that their damping parameter α can be strongly constrained. Furthermore, there are no significant changes in the best-fit neutrino oscillation parameters in these new physics scenarios [30, 31, 33, 40]. The fact that neutrinos are massive implies they could decay. The $n = -1$ case was used in Refs. [13, 16, 18, 38, 55–62] to describe invisible neutrino decay scenarios, which lead to the violation of three-flavor neutrino unitarity. However, Ref. [18] has shown that astrophysical neutrinos are potentially the most powerful source for constraining the decay parameters of ν_1 and ν_2 , which could lead to the lower bounds on $\tau/m \sim 10^{-4}$ (10^6) s/eV from the solar (supernova) neutrinos. Nevertheless, the constraints on ν_3 decay is much weaker than those on ν_1 and ν_2 from the current data [16, 18, 19].

Here, in the type (5) model, we only consider the ν_3 decay scenario [15–17, 19, 41–43]. The oscillation probability of $P(\bar{\nu}_e \rightarrow \bar{\nu}_e)$ comprises two exponential forms derived from the case of $n = -1$, with α being the neutrino eigenstate mass divided by the corresponding lifetime, i.e., $\alpha \equiv m_3/\tau_3$.

Although the plane-wave approximation theory successfully interprets a wide range of neutrino experiments, it is not self-consistent and leads to many paradoxes [46, 51, 52, 63]. Therefore, the models of types (6) - (8) are proposed to form a consistent description of neutrino oscillations, which use the wave packet treatment of neutrino oscillation instead of the plane wave approximation for neutrino propagation [21, 22, 25, 46, 51, 52]. However, this description also induce some WPD effects, which have not been found in current experimental data [22, 24, 49]. Furthermore, the WPD effects and ν_3 decay can shift the best-fit neutrino oscillation parameters if these effects are strong enough [13, 16, 17, 22, 24, 49]. Specifically, the type (6) model is used to describe the decoherence effect caused by wave packet separation [13, 23, 24, 44–49]. This effect is related to the characteristics of the neutrino source and detector. In the type (6) model, $\alpha \equiv 1/(4\sqrt{2}\sigma_x)^2$, where σ_x is the spatial width of the neutrino wave packet. The type (7) model is used in Ref. [50] to show that in the two-neutrino oscillation case, a Gaussian-averaged neutrino oscillation model with $\exp[-2\sigma^2(\Delta m^2)^2]$ and a neutrino decoherence model with $\exp(-d^2L)$ are equivalent if $d = \frac{\sqrt{2}\Delta m^2}{\sqrt{L}}\sigma$ is fulfilled, where σ is the standard deviation of L/E and d is the decoherence parameter. The model with $\exp[-2\sigma^2(\Delta m^2)^2]$ is obtained by Gaussian average over the L/E dependence for the oscillation probability under the plane-wave approximation due to uncertainties in the energy and oscillation length [37, 50]. Since under the condition of $(2\sigma^2 E^4/L^2) = 1/(4\sqrt{2}\sigma_x)^2$, the type (6) and type (7) models are equivalent, we refer to the type (7) model as WPD II.

The type (8) model systematically studies the quantum decoherence effects caused by wave packet separation, dispersion and delocalization. We rewrite the unified decoherence effect in exponential form to discuss its impact on the neutrino oscillation probability. This exponential damping factor is given by [21, 22, 25, 51, 52]

$$\begin{aligned} \exp(-R - \mathbf{i}X) &= \exp\left\{-\left[\frac{1}{4}\ln(1 + y_{ij}^2) + \lambda_{ij} + \eta_{ij}\right] - \mathbf{i}\left[\frac{1}{2}\tan^{-1}(y_{ij}) - \lambda_{ij}y_{ij}\right]\right\} \\ &= \left(\frac{1}{1 + y_{ij}^2}\right)^{\frac{1}{4}} \exp(-\lambda_{ij}) \exp\left(-\frac{\mathbf{i}}{2}\tan^{-1}(y_{ij})\right) \exp(\mathbf{i}\lambda_{ij}y_{ij}) \exp(-\eta_{ij}), \end{aligned} \quad (2.2)$$

where $\lambda_{ij} = \frac{x_{ij}^2}{1+y_{ij}^2}$, $x_{ij} = \frac{\sqrt{2}\Delta m_{ij}^2 L}{4E}\sigma_{\text{rel}}$, $y_{ij} = \frac{\Delta m_{ij}^2 L}{E}\sigma_{\text{rel}}^2$, $\eta_{ij} = \frac{1}{2}\left(\frac{\Delta m_{ij}^2}{4\sigma_{\text{rel}}E^2}\right)^2$, and $\sigma_{\text{rel}} = (2\sigma_x E)^{-1}$. In this model, we define $\alpha \equiv \sigma_{\text{rel}}$, where σ_{rel} represents the intrinsic relative dispersion of neutrino momentum. The $\exp(-\lambda_{ij})$ term corresponds to the conventional quantum decoherence effect caused by the gradual separation of different mass states traveling at different spatial propagation speeds, which causes them to stop interfering with each other, leading to damped oscillations. The terms containing y_{ij} describe the dispersion effect, which includes two effects on the oscillations: wave packet spreading compensates for wave packet separation, and dispersion reduces the overlap fraction of the wave packets [21, 25]. The $\exp(-\eta_{ij})$ term corresponds to the quantum decoherence effect from delocalization, which is related to the neutrino production and detection processes

and is independent of the baseline L . We find that $\exp(-\eta_{ij})$ is very close to 1 at JUNO if $\sigma_{\text{rel}} \gtrsim \mathcal{O}(10^{-15})$. In Ref. [22], the Daya Bay (DYB) collaboration published their first experimental limits, which are $10^{-14} < \sigma_{\text{rel}} < 0.23$ and $2.38 \times 10^{-17} < \sigma_{\text{rel}} < 0.23$ at a 95% CL when the dimensions of the reactor cores and detectors are and are not considered as constraints, respectively. Therefore, we neglect the $\exp(-\eta_{ij})$ term in Eq. (2.2) in this work in the following text*.

In addition, some works have discussed exponential damping models such as $\exp\left(-\alpha \frac{L^2}{(2E)^2}\right)$ and $\exp\left(-\alpha \frac{(\Delta m_{ij}^2)^2 L}{E^2}\right)$. The former was adopted in Ref. [13] to approximately describe the mixing of three active neutrinos and a very light sterile neutrino in short-baseline reactor neutrino experiments. Here, α represents the magnitude of mixing between the three active neutrinos and the light sterile neutrino. Note that this approximate relationship does not hold for medium- or long-baseline neutrino experiments with an eV-scale sterile neutrino or for mixing scenarios involving three active neutrinos and multiple sterile neutrinos. The latter damping model was proposed to explain the decoherence effect caused by quantum gravity in the Super-Kamiokande experiment [64], and the coupling α can be related to M_{Planck} . For a single-baseline experiment or an experiment with multiple identical baselines, the phenomenology of the former model above is the same as that of the type (1) model, and the phenomenology of the latter model above is the same as that of the type (7) model. Therefore, we will not discuss these two models in depth in this paper.

3 Damping signatures at medium-baseline reactor neutrino experiments

In this section, we first discuss the damping effects on the survival probability of $\bar{\nu}_e$ in medium-baseline reactor neutrino experiments. After that, we classify the damping effects in accordance with their different damping behaviors.

3.1 Damped neutrino oscillation probabilities

From the general expression in Eq. (2.1), we can obtain four cases for the damped survival probability of reactor neutrinos ($\bar{\nu}_e$) in vacuum, as follows:

- (I) The overall $\bar{\nu}_e$ survival probability is damped out. This case includes the QD I, QD II, QD III, and absorption damping effects.

$$P(\bar{\nu}_e \rightarrow \bar{\nu}_e) = D \{1 - c_{13}^4 \sin^2(2\theta_{12}) \sin^2(\Delta_{21}) - c_{12}^2 \sin^2(2\theta_{13}) \sin^2(\Delta_{31}) - s_{12}^2 \sin^2(2\theta_{13}) \sin^2(\Delta_{32})\}, \quad (3.1)$$

where the expression in curly brackets represents the $\bar{\nu}_e$ survival probability in vacuum without damping effects (i.e., the standard $\bar{\nu}_e$ survival probability), $D = D_{ij}$ because there are no relevant Δm_{ij}^2 terms in these damping factors, $c_{ij} = \cos \theta_{ij}$, $s_{ij} = \sin \theta_{ij}$, and the

*If we consider the decoherence effect caused by delocalization, the lower limit on σ_{rel} at JUNO can reach 3.0×10^{-17} at 95% CL. Although this expected lower limit is slightly better than the DYB limit of $\sigma_{\text{rel}} > 2.38 \times 10^{-17}$, the improvement from JUNO is not large due to the smaller IBD events compared with DYB and the baseline independence of delocalization [22].

oscillation phase Δ_{ij} is defined as

$$\Delta_{ij} = \frac{\Delta m_{ij}^2 L}{4E} \simeq 1.267 \frac{\Delta m_{ij}^2 [\text{eV}^2] L [\text{km}]}{E [\text{GeV}]} = 1.267 \frac{\Delta m_{ij}^2 [\text{eV}^2] L [\text{m}]}{E [\text{MeV}]}.$$
 (3.2)

(II) Some oscillating and nonoscillating terms of the $\bar{\nu}_e$ survival probability are damped out. This case includes the ν_3 decay damping effect.

$$P(\bar{\nu}_e \rightarrow \bar{\nu}_e) = c_{13}^4 [1 - \sin^2(2\theta_{12}) \sin^2(\Delta_{21})] + \frac{1}{2} \sin^2(2\theta_{13}) \exp\left(-\frac{\alpha L}{2E}\right) [c_{12}^2 \cos(2\Delta_{31}) + s_{12}^2 \cos(2\Delta_{32})] + \exp\left(-\frac{\alpha L}{E}\right) s_{13}^4.$$
 (3.3)

(III) Only the oscillating terms of the $\bar{\nu}_e$ survival probability are damped out, but there are no dispersion terms. This case includes the WPD I and WPD II damping effects.

$$P(\bar{\nu}_e \rightarrow \bar{\nu}_e) = 1 - \frac{1}{2} [c_{13}^4 \sin^2(2\theta_{12}) + \sin^2(2\theta_{13})] + \frac{1}{2} c_{13}^4 \sin^2(2\theta_{12}) D_{21} \cos(2\Delta_{21}) + \frac{1}{2} \sin^2(2\theta_{13}) [D_{31} c_{12}^2 \cos(2\Delta_{31}) + D_{32} s_{12}^2 \cos(2\Delta_{32})].$$
 (3.4)

(IV) Not only are the oscillating terms of the $\bar{\nu}_e$ survival probability damped out, but there are also dispersion terms. This case includes the WPD III damping effect.

$$P(\bar{\nu}_e \rightarrow \bar{\nu}_e) = 1 - \frac{1}{2} c_{13}^4 \sin^2(2\theta_{12}) \left[1 - \left(\frac{1}{1 + y_{21}^2} \right)^{\frac{1}{4}} \exp(-\lambda_{21}) \cos(\phi_{21}) \right] - \frac{1}{2} \sin^2(2\theta_{13}) c_{12}^2 \left[1 - \left(\frac{1}{1 + y_{31}^2} \right)^{\frac{1}{4}} \exp(-\lambda_{31}) \cos(\phi_{31}) \right] - \frac{1}{2} \sin^2(2\theta_{13}) s_{12}^2 \left[1 - \left(\frac{1}{1 + y_{32}^2} \right)^{\frac{1}{4}} \exp(-\lambda_{32}) \cos(\phi_{32}) \right],$$
 (3.5)

where $\phi_{ij} = \frac{\Delta m_{ij}^2 L}{2E} + \frac{1}{2} \arctan(y_{ij}) - \lambda_{ij} y_{ij}$ and is the sum of the plane wave phase and the phase shift introduced by wave packet dispersion.

In general, the $\bar{\nu}_e$ survival probability at JUNO is also affected by the Mikheyev–Smirnov–Wolfenstein (MSW) matter effect as the neutrinos travel through matter [65, 66]. We can treat this damping effect as a minor perturbation of the neutrino oscillations in matter [13]. For the standard three-neutrino oscillation scenarios, the corrections to the neutrino parameters due to matter effects do not exceed 1.1% [11, 67, 68]. In this work, we also ignore matter effects because they only slightly shift the central values of the neutrino oscillation parameters and do not affect the measurement precision.

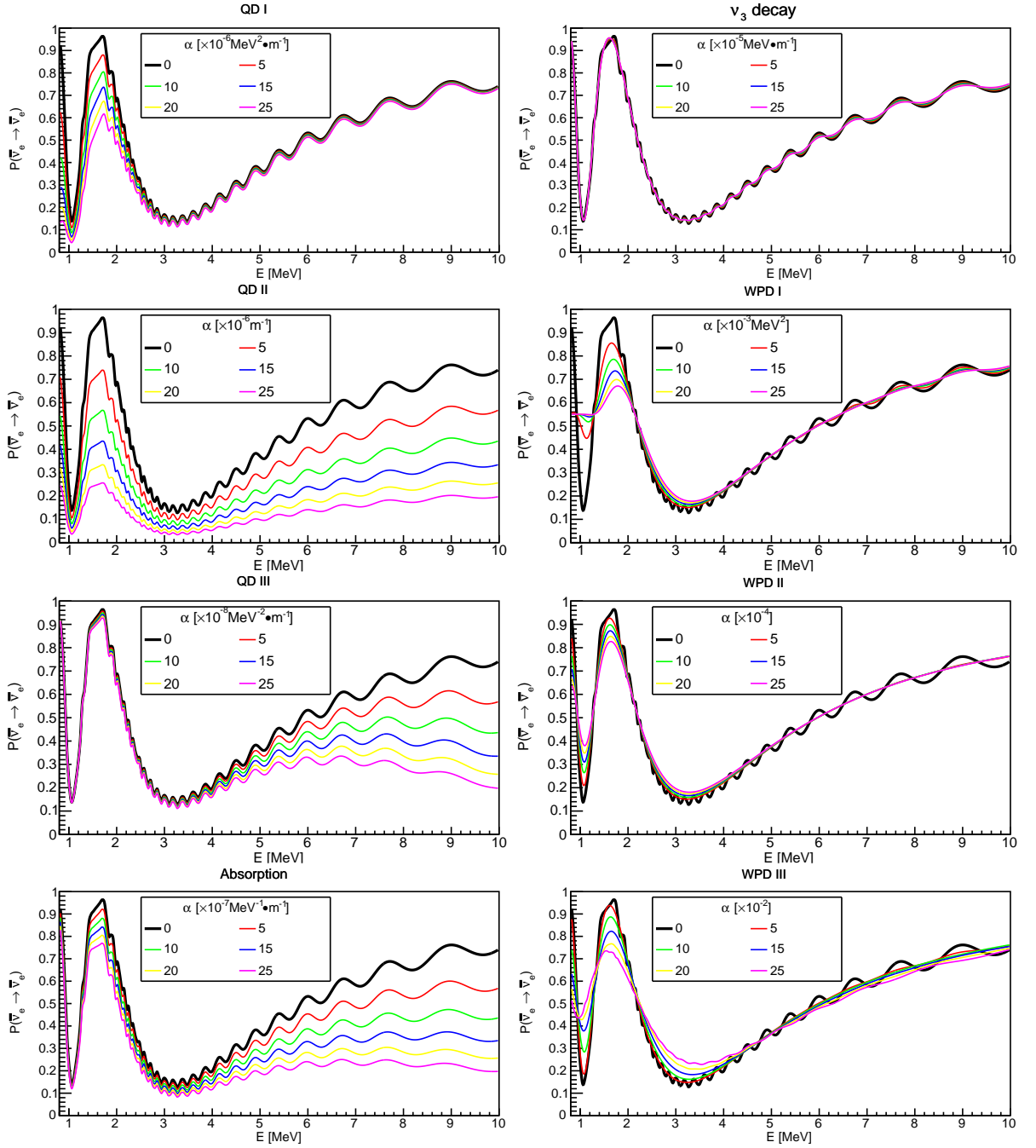


Figure 1: The $\bar{\nu}_e$ survival probability $P(\bar{\nu}_e \rightarrow \bar{\nu}_e)$ with different damping parameter values for each new physics model.

3.2 Classification of damping effects

In Figure 1, we plot the $\bar{\nu}_e$ survival probability $P(\bar{\nu}_e \rightarrow \bar{\nu}_e)$ with different damping parameter values for each new physics model. The neutrino oscillation parameters are taken from Ref. [4] and summarized in Table 2. We assume the NMO in this analysis. We find that the results are

p	$\sin^2 \theta_{12}$	$\sin^2 \theta_{13}$	Δm_{21}^2 (eV ²)	Δm_{32}^2 (NMO, eV ²)	Δm_{32}^2 (IMO, eV ²)
p^{input}	0.307	2.18×10^{-2}	7.53×10^{-5}	2.453×10^{-3}	-2.546×10^{-3}
δp	0.013	0.07×10^{-2}	0.18×10^{-5}	0.034×10^{-3}	0.037×10^{-3}

Table 2: The neutrino oscillation parameters used in this work [4]. The input values p^{input} and the corresponding 1σ uncertainty values δp are taken from Ref. [4]. For the case in which Δm_{32}^2 is negative, the corresponding δp is the average value.

quite similar for the IMO. We choose a few values for the damping parameters for illustration. In particular, $\alpha = 0$ indicates no damping effect, i.e., neutrino oscillation of the standard type. The farther the spectrum is from the no-damping curve, the stronger the intensity of the damping effect. The distortion of the standard $\bar{\nu}_e$ survival probability spectrum caused by damping is a combined phenomenon of an amplitude decrease and a phase shift, which can be regarded as a unique signature, as shown in Figure 1. We find that the amplitude decrease behaviors of both the fast oscillation cycles (driven by Δm_{31}^2 and Δm_{32}^2) and the slow oscillation cycles (driven by Δm_{21}^2) are more significant than their phase shift behaviors in all damping effect scenarios. Therefore, damping effects mainly smear the fine structure of the standard $\bar{\nu}_e$ survival probability spectrum through amplitude-decreasing effects. Furthermore, the fine structure of the fast oscillation cycles is smeared more strongly than that of the slow oscillation cycles with increasing α , which indicates that more spectral shape information is lost in the former than in the latter.

Based on the different smearing behaviors, we can divide the damping effects in Table 1 into three categories. The first category is referred to as the QD-like effects, which include the QD I, QD II, QD III, and absorption damping effects. Although the details of the smearing behavior of each model are different, the fine structure is more completely preserved under increasing α for models in this category than for models in the other two categories. As $\alpha \rightarrow \infty$, the $\bar{\nu}_e$ survival probabilities of the models in this category approach zero, which means that the neutrinos do not propagate. The second category includes the ν_3 decay effect. In this category, the fine structure of the fast oscillation cycles will be smeared more strongly as α increases until all details of the fast oscillation structure are lost. However, the damping effects of this category will not affect the fine structure of the slow oscillation cycles. Consequently, only the slow oscillation cycles will remain as $\alpha \rightarrow \infty$. The third category is referred to as WPD-like effects, which include the WPD I, WPD II, and WPD III damping effects. As α increases, the fine structures of both the fast and slow oscillation cycles will be strongly smeared under WPD-like effects, but the former will be smeared out before the latter. The $\bar{\nu}_e$ survival probabilities of these models approach a nonzero constant value as $\alpha \rightarrow \infty$, i.e., $1 - \frac{1}{2}[c_{13}^4 \sin^2(2\theta_{12}) + \sin^2(2\theta_{13})]$. Notably, the number of neutrinos will be lost in the damping models of the first and second categories, whereas they will keep the same in the third category.

4 Analysis method for JUNO

The damping effects on the reactor neutrino oscillations can be probed at JUNO by measuring the distortion of the neutrino inverse beta decay (IBD) event spectrum. The observed $\bar{\nu}_e$ distribution in terms of the reconstructed energy (E_{rec}) can be expressed as follows [69]:

$$\frac{dN}{dE_{\text{rec}}} = \frac{N_p T}{4\pi L^2} \int_{m_n - m_p + m_e} dE \frac{W_{\text{th}}}{\sum_u f_u \varpi_u} \sum_u f_u S_u(E) P(\bar{\nu}_e \rightarrow \bar{\nu}_e) \sigma_{\text{IBD}}(E) G(E_{\text{vis}} - E_{\text{rec}}, \delta E_{\text{vis}}), \quad (4.1)$$

where N_p is the total number of free target protons in the LS detector, T is the total exposure time, and W_{th} is the thermal power of the reactor. f_u , ϖ_u , and S_u are the fission fraction, the mean energy released per fission, and the $\bar{\nu}_e$ energy spectrum per fission, respectively, for the isotope u , where $u = \{^{235}\text{U}, ^{238}\text{U}, ^{239}\text{Pu}, ^{241}\text{Pu}\}$. The values of f_u and ϖ_u are taken from Ref. [70]. $S_{^{235}\text{U}}$, $S_{^{239}\text{Pu}}$, and $S_{^{241}\text{Pu}}$ are derived from Ref. [71], and $S_{^{238}\text{U}}$ is derived from Ref. [72]. $\sigma_{\text{IBD}}(E)$ is the cross section for IBD in a detector, taken from Refs. [73, 74]; E_{vis} is the visible energy ($E_{\text{vis}} \sim E_e + m_e \sim (E - 0.8) \text{ MeV}$), and $G(E_{\text{vis}} - E_{\text{rec}}, \delta E_{\text{vis}})$ is a normalized Gaussian function representing a detector response function with an energy resolution of δE_{vis} . This function is expressed as follows:

$$G(E_{\text{vis}} - E_{\text{rec}}, \delta E_{\text{vis}}) \approx \frac{1}{\sqrt{2\pi}\delta E_{\text{vis}}} \exp\left\{-\frac{(E_{\text{vis}} - E_{\text{rec}})^2}{2(\delta E_{\text{vis}})^2}\right\}, \quad (4.2)$$

where δE_{vis} is taken from Ref. [11]. The detector energy resolution can be described by a three-parameter function, i.e.,

$$\frac{\delta E_{\text{vis}}}{E_{\text{vis}}} = \sqrt{\left(\frac{p_0}{\sqrt{E_{\text{vis}}/\text{MeV}}}\right)^2 + p_1^2 + \left(\frac{p_2}{E_{\text{vis}}/\text{MeV}}\right)^2}, \quad (4.3)$$

where the parameters p_0 , p_1 and p_2 represent the contributions to the energy resolution from the photon statistics, detector-related residual energy nonuniformity, and photomultiplier tube (PMT)-related effects, respectively.

The effective energy resolution of 3% at 1 MeV of the JUNO detector, as discussed in Refs. [12, 75], is considered, and we set $p_0 = 2.61\%$, $p_1 = 0.82\%$, and $p_2 = 1.23\%$. We also take the IBD detection efficiency of the detector to be 73% [11, 75]. The JUNO detector is located at equal distances of $\sim 53 \text{ km}$ from the Yangjiang and Taishan thermal power reactor complexes [11, 12, 75]. The thermal powers of these two reactor complexes are $17.4 \text{ GW}_{\text{th}}$ and $9.2 \text{ GW}_{\text{th}}$, respectively [75]. We consider the exposure of the JUNO detector to be $(26.6 \times 20 \times 6 \times 300) \text{ GW}_{\text{th}} \cdot \text{kton} \cdot \text{years} \cdot \text{days}$ and assume the NMO scenario unless explicitly stated otherwise.

For the analysis, we adopt the least square method from Refs. [11, 16, 18, 69, 76, 77] and define a χ^2 function with proper nuisance parameters and penalty terms to quantify the sensitivity of α , as follows:

$$\begin{aligned}
\chi^2 = & \sum_i^{N_{\text{bin}}} \frac{[M_i - T_i(1 + \epsilon_R + \epsilon_d + \sum_r \omega_r \epsilon_r + \epsilon_s) - \sum_b B_{b,i}(1 + \epsilon_b)]^2}{T_i + (\sigma^{\text{shape}} T_i)^2 + \sum_b (B_{b,i} \sigma_b^{\text{shape}})^2} \\
& + \frac{\epsilon_R^2}{\sigma_R^2} + \frac{\epsilon_d^2}{\sigma_d^2} + \sum_r \frac{\epsilon_r^2}{\sigma_r^2} + \frac{\epsilon_s^2}{\sigma_s^2} + \sum_b \frac{\epsilon_b^2}{\sigma_b^2} \\
& + \sum_k \left(\frac{p_k^{\text{input}} - p_k^{\text{fit}}}{\delta p_k} \right)^2,
\end{aligned} \tag{4.4}$$

where N_{bin} is the number of energy bins, M_i is the number of measured total events (the summation of signal and background) in the i -th bin, T_i is the predicted number of IBD events, B_b is the b -th kind of estimated background (the main background spectra for the JUNO detector are taken from Ref. [11]), and the quantities σ and ϵ with different indices represent systematic uncertainties and the corresponding pull parameters, respectively. The considered systematic uncertainties include the correlated reactor uncertainty ($\sigma_R=2\%$), the detector-related uncertainty ($\sigma_d=1\%$), the uncorrelated reactor uncertainty ($\sigma_r=0.8\%$), the uncorrelated spectrum shape uncertainty ($\sigma_s=1\%$), the correlated spectrum shape uncertainty ($\sigma^{\text{shape}}=1\%$), the shape uncertainties of the backgrounds (σ_b^{shape}), and the relative rate uncertainties of the backgrounds (σ_b). Specifically, the σ_b^{shape} values for accidental coincidences, fast neutrons, ${}^9\text{Li}/{}^8\text{He}$, ${}^{13}\text{C}(\alpha, n){}^{16}\text{O}$ and geoneutrinos at JUNO are negligible (i.e., 0%), 20%, 10%, 50%, and 5%, respectively; the corresponding σ_b values are 1%, 100%, 20%, 50%, and 30%, respectively. Additionally, ω_r is a fraction representing the r -th reactor's contribution to the corresponding pull parameter ϵ_r . Finally, p_k and δp_k denote the k -th neutrino oscillation parameter ($\sin^2 \theta_{12}$, $\sin^2 \theta_{13}$, Δm_{21}^2 , or Δm_{32}^2) and the corresponding uncertainty, respectively, at a 1σ CL; these values are given in Table 2.

5 Results

In this section, we present the results of probing the damping signatures of different new physics models at JUNO. We firstly study the constraints on the damping parameters for the eight new physics models at JUNO. Then, we show that JUNO can also help to disentangle the damping model from each other.

5.1 Constraints on the damping parameters at JUNO

To obtain the constraints on the damping parameters at JUNO, we scan the damping parameter of each damping model by marginalizing over other parameters, and fit the simulated no-damping JUNO data to obtain the exclusion sensitivities of the damping parameters. We list the constraints on the damping parameter of each damping model from this work in Table 3. The current bounds on the damping parameters in the literature are also listed for comparison. The damping factors of the first seven damping models in Table 3 can be unified into a general form [13, 14],

$$D_{ij} = \exp \left(-\alpha \frac{|\Delta m_{ij}^2|^\xi L^\beta}{E\gamma} \right), \tag{5.1}$$

Damping type Parameter [units]	Phenomenological limits (experiment: original results, CL [Ref]) {Experimental limits (experiment: original results, CL [Ref])}	Exclusion sensitivities for JUNO (CL)
QD I $\alpha [\times 10^{-6} \frac{\text{MeV}^2}{\text{m}}]$	$< 1.62 \times 10^5$ (MINOS+T2K+reactor: $\alpha < 3.2 \times 10^{-23} \text{ GeV}^3$, 90% [33]) < 0.41 (solar+KL: $\alpha < 0.81 \times 10^{-28} \text{ GeV}^3$, 95% [20])	< 3.72 (90%) < 4.42 (95%)
QD II $\alpha [\times \frac{10^{-6}}{\text{m}}]$	< 3.45 (KL: $6.8 \times 10^{-22} \text{ GeV}$, 95% [40]) < 0.33 (MINOS+T2K+reactor: $\alpha < 6.5 \times 10^{-23} \text{ GeV}$, 90% [33]) < 0.18 (SK: $\alpha < 3.5 \times 10^{-23} \text{ GeV}$, 90% [35]) $< 3.40 \times 10^{-3}$ (solar+KL: $\alpha < 0.67 \times 10^{-24} \text{ GeV}$, 95% [20])	< 0.80 (90%) < 0.95 (95%)
QD III $\alpha [\times \frac{10^{-8}}{\text{MeV}^2 \cdot \text{m}}]$	$< 2.38 \times 10^{-3}$ (solar+KL: $\alpha < 0.47 \times 10^{-20} \text{ GeV}^{-1}$, 95% [20]) $< 1.42 \times 10^{-5}$ (MINOS+T2K+reactor: $\alpha < 2.8 \times 10^{-23} \text{ GeV}^{-1}$, 90% [33]) $< 4.56 \times 10^{-10}$ (SK: $\alpha < 0.9 \times 10^{-27} \text{ GeV}^{-1}$, 90% [35])	< 1.22 (90%) < 1.46 (95%)
Absorption $\alpha [\times \frac{10^{-7}}{\text{MeV} \cdot \text{m}}]$	< 7.60 (KL: $\alpha < 1.5 \times 10^{-19}$, 95% [40]) < 0.10 (SK: $\alpha < 2.0 \times 10^{-21}$, 90% [35]) $< 2.94 \times 10^{-3}$ (solar+KL: $\alpha < 0.58 \times 10^{-22}$, 95% [20])	< 1.04 (90%) < 1.23 (95%)
ν_3 decay $\alpha \equiv \frac{m_3}{\tau_3}$ $[\times 10^{-4} \frac{\text{MeV}}{\text{m}}]$	< 256.59 (OPERA: $\frac{\tau_3}{m_3} > 1.3 \times 10^{-13} \frac{\text{s}}{\text{eV}}$, 90% [43]) < 22.24 (NO ν A+T2K: $\frac{\tau_3}{m_3} > 1.5 \times 10^{-12} \frac{\text{s}}{\text{eV}}$, 90% [17]) < 0.36 (SK+K2K+MINOS: $\frac{\tau_3}{m_3} > 9.3 \times 10^{-11} \frac{\text{s}}{\text{eV}}$, 99% [41]) { < 15.88 (MINOS: $\frac{\tau_3}{m_3} > 2.1 \times 10^{-12} \frac{\text{s}}{\text{eV}}$, 90% [15])}	< 0.44 (90%) < 0.53 (95%) < 0.75 (99%)
WPD I $\alpha \equiv (4\sqrt{2}\sigma_x)^{-2}$ $[\times 10^{-3} \text{MeV}^2]$	< 116.96 (RENO+DYB: $\sigma_x > 1.02 \times 10^{-4} \text{ nm}$, 90% [24]) < 27.59 (RENO+DYB+KL: $\sigma_x > 2.1 \times 10^{-4} \text{ nm}$, 90% [49])	< 0.18 (90%) < 0.22 (95%)
WPD II $\alpha [\times 10^{-4}]$		< 0.14 (95%)
WPD III $\alpha \equiv \sigma_{\text{rel}} [\times 10^{-2}]$	{ < 23 (DYB: $\sigma_{\text{rel}} < 0.23$, 95% [22])}	< 1.04 (95%)
$\sigma_x \equiv (2\alpha E)^{-1}$ $[\times 10^{-3} \text{ nm}]$	{ $> 10^{-1}$ (DYB: $\sigma_x > 10^{-4} \text{ nm}$, 95% [22])}	> 2.32 (95%)

Table 3: The limits on the damping parameters for each damping model at JUNO. The experimental and phenomenological limits in the literature are also shown for comparison.

where the parameters ξ , β , and γ are the power numbers in the damping factor of interest. The strength of neutrino oscillation experiments to probe the damping effects is strongly dependent on the specific values of ξ , β , and γ [13, 14].

Compared to current experimental limits, we find that JUNO will improve the limits on τ_3/m_3 in the ν_3 decay model by a factor of ~ 36 . The limits on σ_{rel} (or σ_x) in the WPD III model can be also improved by a factor of ~ 22 (23). After taking into account the previous limits from

phenomenological analysis, we find that JUNO will also impose stronger limits on the damping parameters in WPD I and WPD III. However, the improvement of the bounds on the damping parameters in the QD I, QD II, QD III, ν_3 decay and neutrino absorption scenarios from JUNO is not significant compared to other phenomenological analysis. This is mainly due to the fact that JUNO has a smaller value of $|\Delta m_{ij}^2|^\xi L^\beta/E^\gamma$. From Table 3, we see that a global joint analysis can be more restrictive in terms of these limits, which provides a promising future direction for JUNO to study these damping effects.

In the WPD II model, we also replace α with $(\sqrt{2}\sigma_{\text{rel}}/4)^2$ to study the effect of limit on σ_{rel} in the absence of the quantum decoherence caused by the dispersion effect. We find that the upper limits on σ_{rel} for the WPD II and WPD III are about the same, which means that the quantum decoherence caused by the dispersion effect is negligible on the limits on the damping parameters at JUNO. This can be understood from Figure 2, which shows that the $\bar{\nu}_e$ survival probabilities described by Eq. (3.4) and Eq. (3.5) are very close at JUNO, and the modification to the $\bar{\nu}_e$ survival probability due to the dispersion effect is less than 0.5%.

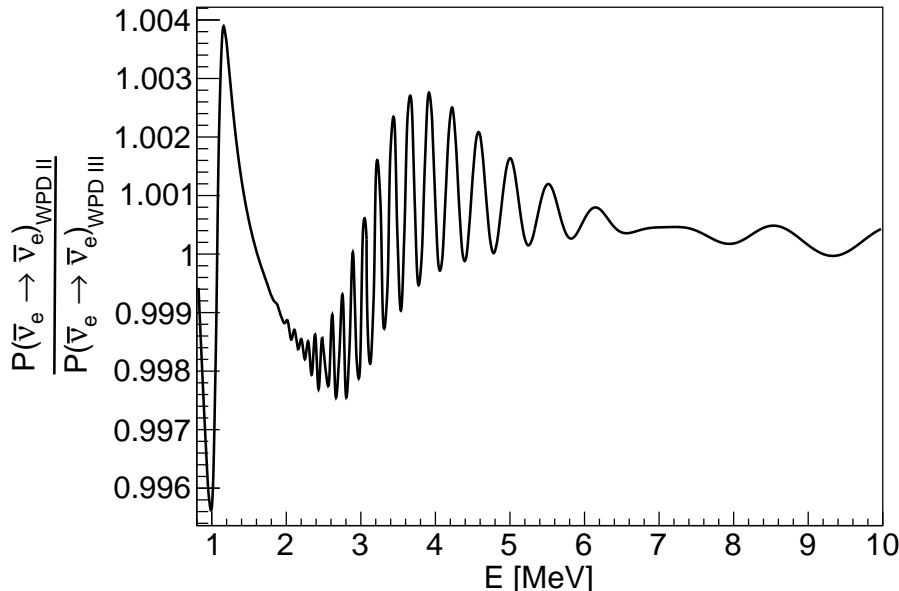


Figure 2: The ratio of the $\bar{\nu}_e$ survival probabilities between the WPD II and WPD III scenarios as a function of the neutrino energy. Here the oscillation parameters are taken from Table 2 and the damping parameter σ_{rel} is set to 2.08×10^{-2} , which corresponds to a 5σ CL limit obtained from this work.

5.2 Disentangling damping signatures at JUNO

To compare these eight damping effects, we follow the analysis method described in Ref. [13]. For a fixed set of oscillation parameters and α values in the simulated damping model, we marginalize over the oscillation parameters, α values and all pull parameters in the fitted model. Then, we define a threshold α_{th} as the sensitivity limit for the simulated α , i.e., the simulated α must be

JUNO 95% (3σ)	Simulated damping model							
Fitted model	QD I $\frac{\alpha}{10^{-6} \frac{\text{MeV}^2}{\text{m}}} \gtrsim$	QD II $\frac{\alpha}{10^{-6} \frac{\text{m}}{\text{m}}} \gtrsim$	QD III $\frac{\alpha}{10^{-8} \frac{\text{MeV}^2 \cdot \text{m}}{\text{m}}} \gtrsim$	Absorption $\frac{\alpha}{10^{-7} \frac{\text{MeV} \cdot \text{m}}{\text{m}}} \gtrsim$	ν_3 decay $\frac{\alpha}{10^{-4} \frac{\text{MeV}}{\text{m}}} \gtrsim$	WPD I $\frac{\alpha}{10^{-3} \text{MeV}^2} \gtrsim$	WPD II $\frac{\alpha}{10^{-4}} \gtrsim$	WPD III $\frac{\alpha}{10^{-2}} \gtrsim$
No damping	4.62 (7.2)	0.99 (1.54)	1.51 (2.35)	1.28 (1.99)	0.55 (0.93)	0.22 (0.44)	0.14 (0.24)	1.05 (1.39)
QD I	-	1.05 (1.62)	1.51 (2.35)	1.28 (1.99)	0.55 (0.93)	0.22 (0.44)	0.14 (0.24)	1.05 (1.39)
QD II	4.82 (7.5)	-	1.75 (2.71)	1.84 (2.84)	0.55 (0.93)	0.22 (0.44)	0.14 (0.24)	1.05 (1.39)
QD III	4.62 (7.2)	1.16 (1.8)	-	4.54 (7.16)	0.55 (0.93)	0.22 (0.44)	0.14 (0.24)	1.05 (1.39)
Absorption	4.62 (7.2)	1.43 (2.24)	5.26 (8.21)	-	0.55 (0.93)	0.22 (0.44)	0.14 (0.24)	1.05 (1.39)
ν_3 decay	4.62 (7.2)	0.99 (1.54)	1.51 (2.35)	1.28 (1.99)	-	4.03 (7.17)	10.48 (16.64)	8.88 (11.04)
WPD I	4.62 (7.2)	0.99 (1.54)	1.51 (2.35)	1.28 (1.99)	4.4 (-)	-	3.2 (39.2)	4.72 (15.68)
WPD II	4.62 (7.2)	0.99 (1.54)	1.51 (2.35)	1.28 (1.99)	-	10 (17.2)	-	21.76 (25.04)
WPD III	4.62 (7.2)	0.99 (1.54)	1.51 (2.35)	1.28 (1.99)	-	9.12 (15.68)	66.8 (88.4)	-

Table 4: The sensitivity limits on α for which a certain simulated damping model (in columns) could be distinguished from a certain fitted model (in rows) at JUNO.

above this threshold for the simulated damping model to be distinguishable from the fitted model at JUNO. The corresponding sensitivity limits at a 95% (3σ) CL obtained through this work are shown in Table 4, where we specifically include the no-damping model among the fitted models. For instance, the QD I model could be distinguished from the no-damping model at the 95% CL if $\alpha \gtrsim 4.62 \times 10^{-6} \text{ MeV}^2/\text{m}$.

In the rows representing ν_3 decay versus WPD-like models, there are no corresponding α_{th} values at the 3σ CL since the χ^2 are below 6.4 for all α values in the simulated ν_3 decay model. This can be attributed to the distortion of the standard $\bar{\nu}_e$ survival probability spectrum caused by the ν_3 decay, which can be easily compensated for by shifting the neutrino oscillation parameters and α in the fitted WPD-like models. In the columns representing WPD-like models, the values with other WPD-like or ν_3 decay scenarios are several orders of magnitude greater than the values with QD-like models. Thus, if a WPD-like model exists in nature, it will be much more difficult

to distinguish it from other WPD-like scenarios or from a ν_3 decay scenario as compared to a QD-like model.

6 Conclusions

In this paper, we systematically study the phenomenology of damping signatures at JUNO, a medium-baseline reactor neutrino oscillation experiment. As the benchmark models in this work, we analyze several new physics scenarios, including quantum decoherence, ν_3 decay, neutrino absorption, and wave packet decoherence. Based on a six-year exposure and five main background sources for the JUNO detector, we demonstrate how to test and disentangle the fine-scale spectral structure caused by the damping effects. The exclusion sensitivities on the damping parameters at JUNO for each benchmark model are listed in Table 3. Compared to current experimental limits, JUNO will significantly improve the limits on τ_3/m_3 in the ν_3 decay model, the width of the neutrino wave packet σ_x , and the intrinsic relative dispersion of neutrino momentum σ_{rel} by a factor of ~ 36 , 23 and 22, respectively. Furthermore, we find that the quantum decoherence caused by the dispersion effect is negligible at JUNO. Finally, we find that compared to the QD-like models, the WPD-like and ν_3 decay models are much more difficult to distinguish from each other at JUNO.

Acknowledgments

We are grateful for the ongoing cooperation from the China General Nuclear Power Group. This work was supported by the Chinese Academy of Sciences, the National Key R&D Program of China, the CAS Center for Excellence in Particle Physics, Wuyi University, and the Tsung-Dao Lee Institute of Shanghai Jiao Tong University in China, the Institut National de Physique Nucléaire et de Physique des Particules (IN2P3) in France, the Istituto Nazionale di Fisica Nucleare (INFN) in Italy, the Italian-Chinese collaborative research program MAECI-NSFC, the Fond de la Recherche Scientifique (F.R.S-FNRS) and FWO under the “Excellence of Science – EOS” in Belgium, the Conselho Nacional de Desenvolvimento Científico e Tecnológico in Brazil, the Agencia Nacional de Investigación y Desarrollo in Chile, the Charles University Research Centre and the Ministry of Education, Youth, and Sports in Czech Republic, the Deutsche Forschungsgemeinschaft (DFG), the Helmholtz Association, and the Cluster of Excellence PRISMA+ in Germany, the Joint Institute of Nuclear Research (JINR) and Lomonosov Moscow State University in Russia, the joint Russian Science Foundation (RSF) and National Natural Science Foundation of China (NSFC) research program, the MOST and MOE in Taiwan, the Chulalongkorn University and Suranaree University of Technology in Thailand, and the University of California at Irvine in USA.

References

- [1] B. Pontecorvo, *Inverse beta processes and nonconservation of lepton charge*, Zh. Eksp. Teor. Fiz. **34** (1957) 247. [*Sov. Phys. JETP*, 7 (1958), pp. 172-173].
- [2] **Super-Kamiokande** Collaboration, Y. Fukuda et al., *Evidence for oscillation of atmospheric neutrinos*, Phys. Rev. Lett. **81** (1998) 1562–1567, [[hep-ex/9807003](#)].

- [3] C. Giganti, S. Lavignac, and M. Zito, *Neutrino oscillations: The rise of the PMNS paradigm*, Prog. Part. Nucl. Phys. **98** (2018) 1–54, [[arXiv:1710.00715](#)].
- [4] **Particle Data Group** Collaboration, P. A. Zyla et al., *Review of Particle Physics*, PTEP **2020** (2020), no. 8 083C01.
- [5] **NOvA** Collaboration, P. Adamson et al., *Measurement of the neutrino mixing angle θ_{23} in NOvA*, Phys. Rev. Lett. **118** (2017), no. 15 151802, [[arXiv:1701.05891](#)].
- [6] **Super-Kamiokande** Collaboration, K. Abe et al., *Atmospheric neutrino oscillation analysis with external constraints in Super-Kamiokande I-IV*, Phys. Rev. D **97** (2018), no. 7 072001, [[arXiv:1710.09126](#)].
- [7] **T2K** Collaboration, K. Abe et al., *Constraint on the matter–antimatter symmetry-violating phase in neutrino oscillations*, Nature **580** (2020), no. 7803 339–344, [[arXiv:1910.03887](#)]. [Erratum: Nature 583, E16 (2020)].
- [8] **DUNE** Collaboration, R. Acciarri et al., *Long-Baseline Neutrino Facility (LBNF) and Deep Underground Neutrino Experiment (DUNE): Conceptual Design Report, Volume 2: The Physics Program for DUNE at LBNF*, [arXiv:1512.06148](#).
- [9] **DUNE** Collaboration, B. Abi et al., *Long-baseline neutrino oscillation physics potential of the DUNE experiment*, Eur. Phys. J. C **80** (2020), no. 10 978, [[arXiv:2006.16043](#)].
- [10] **Hyper-Kamiokande** Collaboration, K. Abe et al., *Hyper-Kamiokande Design Report*, [arXiv:1805.04163](#).
- [11] **JUNO** Collaboration, F. An et al., *Neutrino Physics with JUNO*, J. Phys. G **43** (2016), no. 3 030401, [[arXiv:1507.05613](#)].
- [12] **JUNO** Collaboration, A. Abusleme et al., *JUNO Physics and Detector*, [arXiv:2104.02565](#).
- [13] M. Blennow, T. Ohlsson, and W. Winter, *Damping signatures in future neutrino oscillation experiments*, JHEP **06** (2005) 049, [[hep-ph/0502147](#)].
- [14] M. Blennow, *Damping signatures in future neutrino oscillation experiments*, Nucl. Phys. B Proc. Suppl. **155** (2006) 195–196.
- [15] **MINOS** Collaboration, P. Adamson et al., *Search for sterile neutrino mixing in the MINOS long baseline experiment*, Phys. Rev. D **81** (2010) 052004, [[arXiv:1001.0336](#)].
- [16] T. Abrahão, H. Minakata, H. Nunokawa, and A. A. Quiroga, *Constraint on Neutrino Decay with Medium-Baseline Reactor Neutrino Oscillation Experiments*, JHEP **11** (2015) 001, [[arXiv:1506.02314](#)].
- [17] S. Choubey, D. Dutta, and D. Pramanik, *Invisible neutrino decay in the light of NOvA and T2K data*, JHEP **08** (2018) 141, [[arXiv:1805.01848](#)].
- [18] Y. P. Porto-Silva, S. Prakash, O. L. G. Peres, H. Nunokawa, and H. Minakata, *Constraining visible neutrino decay at KamLAND and JUNO*, Eur. Phys. J. C **80** (2020), no. 10 999, [[arXiv:2002.12134](#)].
- [19] A. Ghoshal, A. Giarnetti, and D. Meloni, *Neutrino Invisible Decay at DUNE: a multi-channel analysis*, J. Phys. G **48** (2021), no. 5 055004, [[arXiv:2003.09012](#)].
- [20] G. L. Fogli, E. Lisi, A. Marrone, D. Montanino, and A. Palazzo, *Probing non-standard decoherence effects with solar and KamLAND neutrinos*, Phys. Rev. D **76** (2007) 033006, [[arXiv:0704.2568](#)].

- [21] Y.-L. Chan, M. C. Chu, K. M. Tsui, C. F. Wong, and J. Xu, *Wave-packet treatment of reactor neutrino oscillation experiments and its implications on determining the neutrino mass hierarchy*, Eur. Phys. J. C **76** (2016), no. 6 310, [[arXiv:1507.06421](#)].
- [22] **Daya Bay** Collaboration, F. P. An et al., *Study of the wave packet treatment of neutrino oscillation at Daya Bay*, Eur. Phys. J. C **77** (2017), no. 9 606, [[arXiv:1608.01661](#)].
- [23] J. A. B. Coelho, W. A. Mann, and S. S. Bashar, *Nonmaximal θ_{23} mixing at NOvA from neutrino decoherence*, Phys. Rev. Lett. **118** (2017), no. 22 221801, [[arXiv:1702.04738](#)].
- [24] A. de Gouvea, V. de Romeri, and C. A. Ternes, *Probing neutrino quantum decoherence at reactor experiments*, JHEP **08** (2020) 018, [[arXiv:2005.03022](#)].
- [25] Z. Cheng, W. Wang, C. F. Wong, and J. Zhang, *Studying the neutrino wave-packet effects at medium-baseline reactor neutrino oscillation experiments and the potential benefits of an extra detector*, Nucl. Phys. B **964** (2021) 115304, [[arXiv:2009.06450](#)].
- [26] Y. Liu, J.-L. Chen, and M.-L. Ge, *A Constraint on EHNS parameters from solar neutrino problem*, J. Phys. G **24** (1998) 2289–2296, [[hep-ph/9711381](#)].
- [27] S. Shafaq, T. Kushwaha, and P. Mehta, *Investigating Leggett-Garg inequality in neutrino oscillations – role of decoherence and decay*, [[arXiv:2112.12726](#)].
- [28] N. C. Ribeiro, H. Nunokawa, T. Kajita, S. Nakayama, P. Ko, and H. Minakata, *Probing Nonstandard Neutrino Physics by Two Identical Detectors with Different Baselines*, Phys. Rev. D **77** (2008) 073007, [[arXiv:0712.4314](#)].
- [29] Y. Farzan, T. Schwetz, and A. Y. Smirnov, *Reconciling results of LSND, MiniBooNE and other experiments with soft decoherence*, JHEP **07** (2008) 067, [[arXiv:0805.2098](#)].
- [30] P. A. N. Machado, H. Nunokawa, F. A. Pereira dos Santos, and R. Zukanovich Funchal, *Testing Nonstandard Neutrino Properties with a Mössbauer Oscillation Experiment*, JHEP **11** (2011) 136, [[arXiv:1108.3339](#)].
- [31] R. L. N. de Oliveira, M. M. Guzzo, and P. C. de Holanda, *Quantum Dissipation and CP Violation in MINOS*, Phys. Rev. D **89** (2014), no. 5 053002, [[arXiv:1401.0033](#)].
- [32] P. Coloma, J. Lopez-Pavon, I. Martinez-Soler, and H. Nunokawa, *Decoherence in Neutrino Propagation Through Matter, and Bounds from IceCube/DeepCore*, Eur. Phys. J. C **78** (2018), no. 8 614, [[arXiv:1803.04438](#)].
- [33] A. L. G. Gomes, R. A. Gomes, and O. L. G. Peres, *Quantum decoherence and relaxation in neutrinos using long-baseline data*, [[arXiv:2001.09250](#)].
- [34] Y. Liu, L.-z. Hu, and M.-L. Ge, *The Effect of quantum mechanics violation on neutrino oscillation*, Phys. Rev. D **56** (1997) 6648–6652.
- [35] E. Lisi, A. Marrone, and D. Montanino, *Probing possible decoherence effects in atmospheric neutrino oscillations*, Phys. Rev. Lett. **85** (2000) 1166–1169, [[hep-ph/0002053](#)].
- [36] D. Morgan, E. Winstanley, J. Brunner, and L. F. Thompson, *Probing quantum decoherence in atmospheric neutrino oscillations with a neutrino telescope*, Astropart. Phys. **25** (2006) 311–327, [[astro-ph/0412618](#)].
- [37] N. E. Mavromatos and S. Sarkar, *Methods of approaching decoherence in the flavour sector due to space-time foam*, Phys. Rev. D **74** (2006) 036007, [[hep-ph/0606048](#)].
- [38] P. Mehta and W. Winter, *Interplay of energy dependent astrophysical neutrino flavor ratios and new physics effects*, JCAP **03** (2011) 041, [[arXiv:1101.2673](#)].

- [39] P. Bakhti, Y. Farzan, and T. Schwetz, *Revisiting the quantum decoherence scenario as an explanation for the LSND anomaly*, JHEP **05** (2015) 007, [[arXiv:1503.05374](#)].
- [40] G. Balieiro Gomes, M. M. Guzzo, P. C. de Holanda, and R. L. N. Oliveira, *Parameter Limits for Neutrino Oscillation with Decoherence in KamLAND*, Phys. Rev. D **95** (2017), no. 11 113005, [[arXiv:1603.04126](#)].
- [41] M. C. Gonzalez-Garcia and M. Maltoni, *Status of Oscillation plus Decay of Atmospheric and Long-Baseline Neutrinos*, Phys. Lett. B **663** (2008) 405–409, [[arXiv:0802.3699](#)].
- [42] R. A. Gomes, A. L. G. Gomes, and O. L. G. Peres, *Constraints on neutrino decay lifetime using long-baseline charged and neutral current data*, Phys. Lett. B **740** (2015) 345–352, [[arXiv:1407.5640](#)].
- [43] G. Pagliaroli, N. Di Marco, and M. Mannarelli, *Enhanced tau neutrino appearance through invisible decay*, Phys. Rev. D **93** (2016), no. 11 113011, [[arXiv:1603.08696](#)].
- [44] C. Giunti, C. W. Kim, and U. W. Lee, *Coherence of neutrino oscillations in vacuum and matter in the wave packet treatment*, Phys. Lett. B **274** (1992) 87–94.
- [45] C. Giunti and C. W. Kim, *Coherence of neutrino oscillations in the wave packet approach*, Phys. Rev. D **58** (1998) 017301, [[hep-ph/9711363](#)].
- [46] C. Giunti, *Coherence and wave packets in neutrino oscillations*, Found. Phys. Lett. **17** (2004) 103–124, [[hep-ph/0302026](#)].
- [47] M. Blasone, F. Dell’Anno, S. De Siena, and F. Illuminati, *Flavor entanglement in neutrino oscillations in the wave packet description*, EPL **112** (2015), no. 2 20007, [[arXiv:1510.06761](#)].
- [48] J. Kersten and A. Y. Smirnov, *Decoherence and oscillations of supernova neutrinos*, Eur. Phys. J. C **76** (2016), no. 6 339, [[arXiv:1512.09068](#)].
- [49] A. de Gouvêa, V. De Romeri, and C. A. Ternes, *Combined analysis of neutrino decoherence at reactor experiments*, JHEP **06** (2021) 042, [[arXiv:2104.05806](#)].
- [50] T. Ohlsson, *Equivalence between neutrino oscillations and neutrino decoherence*, Phys. Lett. B **502** (2001) 159–166, [[hep-ph/0012272](#)].
- [51] D. V. Naumov and V. A. Naumov, *A Diagrammatic treatment of neutrino oscillations*, J. Phys. G **37** (2010) 105014, [[arXiv:1008.0306](#)].
- [52] D. V. Naumov and V. A. Naumov, *Quantum Field Theory of Neutrino Oscillations*, Phys. Part. Nucl. **51** (2020), no. 1 1–106.
- [53] J. R. Ellis, N. E. Mavromatos, D. V. Nanopoulos, and E. Winstanley, *Quantum decoherence in a four-dimensional black hole background*, Mod. Phys. Lett. A **12** (1997) 243–256, [[gr-qc/9602011](#)].
- [54] J. R. Ellis, N. E. Mavromatos, and D. V. Nanopoulos, *Quantum decoherence in a D foam background*, Mod. Phys. Lett. A **12** (1997) 1759–1773, [[hep-th/9704169](#)].
- [55] M. Lindner, T. Ohlsson, and W. Winter, *A Combined treatment of neutrino decay and neutrino oscillations*, Nucl. Phys. B **607** (2001) 326–354, [[hep-ph/0103170](#)].
- [56] A. S. Joshipura, E. Masso, and S. Mohanty, *Constraints on decay plus oscillation solutions of the solar neutrino problem*, Phys. Rev. D **66** (2002) 113008, [[hep-ph/0203181](#)].
- [57] J. F. Beacom and N. F. Bell, *Do Solar Neutrinos Decay?*, Phys. Rev. D **65** (2002) 113009, [[hep-ph/0204111](#)].

- [58] G. L. Fogli, E. Lisi, A. Marrone, and D. Montanino, *Status of atmospheric $\nu(\mu) \rightarrow \nu(\tau)$ oscillations and decoherence after the first K2K spectral data*, Phys. Rev. D **67** (2003) 093006, [[hep-ph/0303064](#)].
- [59] P. Baerwald, M. Bustamante, and W. Winter, *Neutrino Decays over Cosmological Distances and the Implications for Neutrino Telescopes*, JCAP **10** (2012) 020, [[arXiv:1208.4600](#)].
- [60] R. Picoreti, M. M. Guzzo, P. C. de Holanda, and O. L. G. Peres, *Neutrino Decay and Solar Neutrino Seasonal Effect*, Phys. Lett. B **761** (2016) 70–73, [[arXiv:1506.08158](#)].
- [61] A. M. Gago, R. A. Gomes, A. L. G. Gomes, J. Jones-Perez, and O. L. G. Peres, *Visible neutrino decay in the light of appearance and disappearance long baseline experiments*, JHEP **11** (2017) 022, [[arXiv:1705.03074](#)].
- [62] **SNO** Collaboration, B. Aharmim et al., *Constraints on Neutrino Lifetime from the Sudbury Neutrino Observatory*, Phys. Rev. D **99** (2019), no. 3 032013, [[arXiv:1812.01088](#)].
- [63] E. K. Akhmedov and A. Y. Smirnov, *Paradoxes of neutrino oscillations*, Phys. Atom. Nucl. **72** (2009) 1363–1381, [[arXiv:0905.1903](#)].
- [64] S. L. Adler, *Comment on a proposed Super-Kamiokande test for quantum gravity induced decoherence effects*, Phys. Rev. D **62** (2000) 117901, [[hep-ph/0005220](#)].
- [65] L. Wolfenstein, *Neutrino Oscillations in Matter*, Phys. Rev. D **17** (1978) 2369–2374.
- [66] S. P. Mikheyev and A. Y. Smirnov, *Resonance Amplification of Oscillations in Matter and Spectroscopy of Solar Neutrinos*, Sov. J. Nucl. Phys. **42** (1985) 913–917.
- [67] Y.-F. Li, Y. Wang, and Z.-z. Xing, *Terrestrial matter effects on reactor antineutrino oscillations at JUNO or RENO-50: how small is small?*, Chin. Phys. C **40** (2016), no. 9 091001, [[arXiv:1605.00900](#)].
- [68] A. N. Khan, H. Nunokawa, and S. J. Parke, *Why matter effects matter for JUNO*, Phys. Lett. B **803** (2020) 135354, [[arXiv:1910.12900](#)].
- [69] S.-F. Ge, K. Hagiwara, N. Okamura, and Y. Takaesu, *Determination of mass hierarchy with medium baseline reactor neutrino experiments*, JHEP **05** (2013) 131, [[arXiv:1210.8141](#)].
- [70] **Daya Bay** Collaboration, F. P. An et al., *Improved Measurement of the Reactor Antineutrino Flux and Spectrum at Daya Bay*, Chin. Phys. C **41** (2017), no. 1 013002, [[arXiv:1607.05378](#)].
- [71] P. Huber, *On the determination of anti-neutrino spectra from nuclear reactors*, Phys. Rev. C **84** (2011) 024617, [[arXiv:1106.0687](#)]. [Erratum: Phys.Rev.C **85**, 029901 (2012)].
- [72] T. A. Mueller et al., *Improved Predictions of Reactor Antineutrino Spectra*, Phys. Rev. C **83** (2011) 054615, [[arXiv:1101.2663](#)].
- [73] A. Strumia and F. Vissani, *Precise quasielastic neutrino/nucleon cross-section*, Phys. Lett. B **564** (2003) 42–54, [[astro-ph/0302055](#)].
- [74] A. S. Dighe, M. T. Keil, and G. G. Raffelt, *Detecting the neutrino mass hierarchy with a supernova at IceCube*, JCAP **06** (2003) 005, [[hep-ph/0303210](#)].
- [75] **JUNO** Collaboration, A. Abusleme et al., *Calibration Strategy of the JUNO Experiment*, JHEP **03** (2021) 004, [[arXiv:2011.06405](#)].
- [76] F. Capozzi, E. Lisi, and A. Marrone, *Neutrino mass hierarchy and electron neutrino oscillation parameters with one hundred thousand reactor events*, Phys. Rev. D **89** (2014), no. 1 013001, [[arXiv:1309.1638](#)].

- [77] H. Wang, L. Zhan, Y.-F. Li, G. Cao, and S. Chen, *Mass hierarchy sensitivity of medium baseline reactor neutrino experiments with multiple detectors*, Nucl. Phys. B **918** (2017) 245–256, [[arXiv:1602.04442](#)].